# An Open Set Domain Adaptation Algorithm via Exploring Transferability and Discriminability for Remote Sensing Image Scene Classification

Jun Zhang, Jiao Liu, Bin Pan, Zongqing Chen, Xia Xu and Zhenwei Shi

**Abstract**

Remote sensing image scene classification aims to automatically assign semantic labels for remote sensing images. Recently, to overcome the distribution discrepancy of training data and test data, domain adaptation has been applied to remote sensing image scene classification. Most domain adaptation approaches usually explore transferability under the assumption that the source domain and target domain have common classes. However, in real applications, new categories may appear in the target domain. Besides, only considering the transferability will degrade the classification performance due to the strong inter-class similarity of remote sensing images. In this paper, we present an open set domain adaptation algorithm via exploring transferability and discriminability (OSDA-ETD) for remote sensing image scene classification. To be specific, we propose the transferability technology, which aims at the high inter-domain variations and high intra-class diversity of remote sensing images. The purpose of transferability is to reduce the global distribution difference of domains and the local distribution discrepancy of the same classes in different domains. For high inter-class similarity in remote sensing images, we adopt the discriminability strategy. The discriminability intends to enlarge the distribution discrepancy of different classes in different domains. To further promote the effectiveness of scene classification, we integrate the transferability and the discriminability into a framework. Moreover, we prove that the algorithm has a unique optimizer.

**Index Terms**

This work was supported by the National Key R&D Program of China under the Grant 2019YFC1510900, the National Natural Science Foundation of China under the Grant 62001251,62001252 and 61902106, the China Postdoctoral Science Foundation under the Grant 2020M670631, the Natural Science Foundation of Tianjin under the Grant 19JCZDJC40000, the Natural Science Foundation of Hebei province of China under the Grant F2020202008 and the Scientific and Technological Research Project of Hebei Province Universities and Colleges under the Grant ZD2021311. *(Corresponding author: Bin Pan.)*

Jun Zhang and Jiao Liu are with the School of Artificial Intelligence, Hebei University of Technology, Tianjin 300401, China, and also with the Hebei Province Key Laboratory of Big Data Calculation, Tianjin 300401, China (e-mail:zhangjun@scse.hebut.edu.cn; liujiao.hebut@hotmail.com).

Bin Pan and Zongqing Chen are with the School of Statistics and Data Science, Nankai University, Tianjin 300071, China, and also with the Key Laboratory of Pure Mathematics and Combinatorics, Ministry of Education,China (e-mail: panbin@nankai.edu.cn, zqchern@nankai.edu.cn).

Xia Xu is with the College of Computer Science, Nankai University, Tianjin 300350, China. (e-mail: xuxia@nankai.edu.cn).

Zhenwei Shi is with the Image Processing Center, School of Astronautics, Beihang University, Beijing 100191, China (e-mail: shizhenwei@buaa.edu.cn).

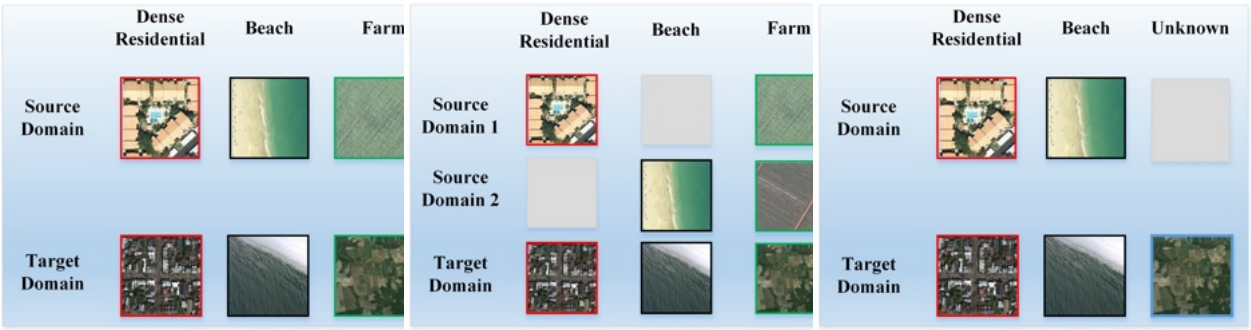


(a) $\mathcal{Y}_t = \mathcal{Y}_s$ (b) $\mathcal{Y}_t = \cup_{k=1}^{K} \mathcal{Y}_{sk}$ (c) $\mathcal{Y}_t \supset \mathcal{Y}_s$

Fig. 1. Different domain adaptation scenarios, where grey modules indicate that this class is absent in the domain. (a). It assumes that the source domain and the target domain have common categories, where $\mathcal{Y}_t$ denotes the target domain label space and $\mathcal{Y}_s$ denotes the source domain label space. (b). The target domain and the combination of multiple-source domains share the same categories, where $\mathcal{Y}_{sk}$ denotes the label space in kth source domain. (c). This is the scenario of open set domain adaptation, and the target domain includes unknown classes.

Remote sensing, Scene classification, Open set domain adaptation, Transferability, Discriminablity.

## I. Introduction

The purpose of remote sensing image scene classification is to assign each image with a specific semantic label, which has been widely applied to urban planning, environmental monitoring, geographic image retrieval [1]–[3]. In recent years, many deep learning approaches have been proposed for scene classification, such as autoencoder-based [4], [5], convolutional neural networks-based [6]–[8], and generative adversarial networks-based methods [9]–[11].

The previous methods assume that the training and the test data are drawn from the same distribution [12]. However, this assumption is hard to guarantee in remote sensing. Remote sensing images are taken under different conditions. Sensor types, resolutions, geographic locations, and other factors can cause distribution discrepancy between the training and the test data [13], [14]. To deal with this problem, domain adaptation has been introduced, which aims to reduce the distribution discrepancy between the labeled data (source domain) and the unlabeled data ( target domain) [15].

In remote sensing scene classification, based on the number of available source domains, domain adaptation can be roughly divided into the single-source domain and multi-source domain adaptation methods. The single-source domain adaptation means that there is one available source domain. In single-source domain adaptation, the source domain and target domain have common classes, but the data distribution is different, as shown in Fig. 1 (a). The literatures [16]–[20] design domain adaptive algorithm to reduce the global or local distribution difference between domains. Recently, to improve the classification performance of the target domain, multi-source domain adaptation has been proposed. In multi-source domain adaptation, there have multiple source domains. The literature [21] proposes a situation that multiple source domains and target domain have the common classes and designs a multi-branch neural network to learn invariant feature between domains. To further deal with the case that the target domain has more classes than any single source domain. Recently, the literature [22] utilizes multiple complementary source domains to combine the classes of target domain, as shown in Fig. 1 (b), and proposes the multi-source compensation network to mitigates the domain shifts.

However, it still has the following two bottlenecks in the domain adaptation of scene classification:

- It is difficult to ensure that the source domain and the target domain have common classes. The new classes will inevitably appear in the target domain.
- The traditional domain adaptation methods reduce the global difference of inter-domain or the local discrepancy of intra-class to improve transferability. When small inter-class variations occur, only improving transferability may deteriorate the decision boundary.

To cope with the first challenges, a novel scenario of an open set domain adaptation has been proposed. As shown in Fig. 1 (c), the target domain contains unknown classes that do not present in the source domain. In the literature [23], the proposed semisupervised dual-dictionary nonnegative matrix factorization algorithm is extended to open set domain adaptation for hyperspectral image classification. In computer vision, the literatures [24]–[26] achieve open set domain adaptation via recognizing unknown classes and improving the transferability of inter-domain or intra-class. However, the low inter-class discrepancy of remote sensing images determines that only considering the transferability will degrade the classification performance.

In this paper, to address the above-mentioned challenges, we present an open set domain adaptation algorithm via exploring transferability and discriminability (OSDA-ETD) for remote sensing image scene classification. As shown in Fig.2, based on the remote sensing images characteristics of large inter-domain variations, large intra-class diversity, and small inter-class discrepancy, OSDA-ETD adopts two strategies. The first technology is transferability, which not only minimizes the global distribution discrepancy between domains, but also reduces the local distribution difference of the same class in different domains. The second strategy is discriminability, which tries to maximize the distribution difference of different categories in different domains. Finally, we embed the transferability and discriminability into a framework, and provide theoretical proof about the optimizer.

The main contributions of this paper are summarized as follows.

- We present a new open set domain adaptation algorithm called OSDA-ETD, which considers the remote sensing images characteristics of large inter-domain variations, large intra-class diversity, and large inter-class similarity.
- Aiming at the remote sensing characteristics, we propose the transferability and discriminability strategy, and prove that the OSDA-ETD has a unique optimizer.

The remainder of this paper is structured as follows. In section II, we introduce the proposed method in detail. In section III, we conduct experiments on cross-domain data sets. Section IV concludes this paper.

## II. Methodology

### A. Open Set Domain Adaptation

In open set domain adaptation, let us define $\mathcal{D}_s = \left\{\mathbf{x}_{s_i}, \mathrm{y}_{s_i}\right\}_{i=1}^{n_s}$ as the labeled source domain and $\mathcal{D}_t = \left\{\mathbf{x}_{t_j}\right\}_{j=1}^{n_t}$ as the unlabeled target domain. $\mathcal{Y}_s = \{\mathbf{y}_c\}_{c=1}^{C}$ denotes the label space of the source domain and $\mathcal{Y}_t = \{\mathbf{y}_{\hat{c}}\}_{\hat{c}=1}^{C+1}$ denotes the label space of target domain. The relationship of label set between the source domain and target domain can be expressed as $\mathcal{Y}_s \subset \mathcal{Y}_t$. Generally speaking, the known classes refer to the shared classes between domains while the unknown classes is the private classes of target domain. In addition, the marginal distribution of source

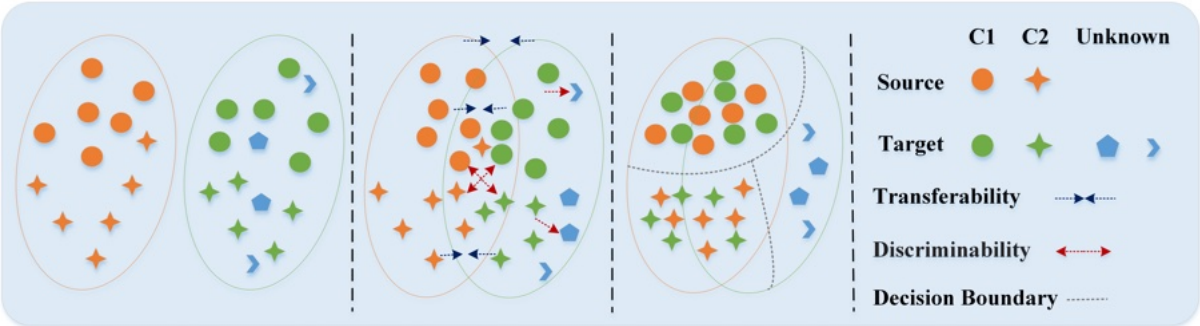


Fig. 2. The motivation and strategy diagram of OSDA-ETD. In the left column, the source domain and the target domain show the characteristics of large inter-domain variations, large intra-class diversity, and small inter-class discrepancy. In the second column, the proposed method not only improves the transferability of inter-domain and inter-class, but also enhances the discriminability of inter-class. In the third column, with the proposed method, the same class can be well aligned and different classes are more discriminative. The right column represents the legend.

TABLE I: NOTATIONS AND THEIR DESCRIPTIONS IN THIS PAPER.

| Notation | Description |
|---|---|
| $\mathcal{D}_s$,$\mathcal{D}_t$ | source, target domain |
| $\mathcal{Y}_s$,$\mathcal{Y}_t$ | source, target label space |
| $\mathbf{x}_{s_i}$,$\mathbf{x}_{t_j}$ | source, target samples |
| $\mathbf{x}_{t_j}^k$ | the predicted known target samples |
| $n_s$,$n_t$ | the number of source or target samples |
| $n_t^k$ | the number of predicted known target samples |
| $n_s^c$ | the number of source samples with label c |
| $n_t^{\hat{c}}$ | the number of target samples with pseudo label $\hat{c}$ |
| $C$ | the number of known classes |
| $C+1$ | the number of target domain classes |
| $Q_s$ | source domain marginal distribution |
| $Q_t^{\mathcal{Y}_s}$ | known classes marginal distribution in target domain |
| $Q_s^{\mathbf{x}_s\|\mathbf{y}_c}$,$Q_t^{\mathbf{x}_t\|\mathbf{y}_{\hat{c}}}$ | source, target conditional distribution |
| $\lambda, \alpha, \eta, \gamma, \sigma, \mu, \rho, p$ | parameters |
| $\boldsymbol{\theta}$ | parameter |
| $K$ | kernel |
| $\mathbf{Y}, \tilde{\mathbf{Y}}$ | label matrix |

domain and target domain is $Q_s$ and $Q_t$ respectively. In the standard domain adaptation, we have $Q_s \neq Q_t$. In open set domain adaptation, we further have $Q_s \neq Q_t^{\mathcal{Y}_s}$ and $Q_s^{\mathbf{x}_s|\mathbf{y}_c} \neq Q_t^{\mathbf{x}_t|\mathbf{y}_{\hat{c}}}$. In this paper, $Q_t^{\mathcal{Y}_s}$ denotes the marginal distribution of the known classes in target domain, $Q_s^{\mathbf{x}_s|\mathbf{y}_c}$ and $Q_t^{\mathbf{x}_t|\mathbf{y}_{\hat{c}}}$represent the class conditional distribution of source domain and target domain respectively.

Notably, some frequently used notations and their corresponding descriptions are listed in Table I. Then we will present the proposed approach.

### *B. General Framework of OSDA-ETD*

In computer vision, Fang *et al.* [25] designs distribution alignment with open difference (DAOD) to solve open set domain adaptation. However, DAOD can not get advanced results for remote sensing images. The reason is

that remote sensing images have the characteristic of high inter-domain variations, high intra-class diversity, and low inter-class discrepancy. In this paper, we propose OSDA-ETD for remote sensing image scene classification. Peculiarly, OSDA-ETD tries to optimize four complementary objective as follows:

(1) In open set domain adaptation, the labeled source domain and the unlabled target domain have different classes. To identify known classes, OSDA-ETD minimizes the source domain structure risk. For the unknown classes, based on DAOD, OSDA-ETD minimizes open set difference.

(2) Aiming at the remote sensing images characteristic of high inter-domain variations and high intra-class diversity, OSDA-ETD adopts the transferability strategy, which can reduce the global inter-domain difference and the local intra-class discrepancy.

(3) For the remote sensing images characteristic of low inter-class discrepancy, OSDA-ETD utilizes the discriminability strategy, which can enhance the inter-class difference in different domains.

(4) Maximizing the manifold consistency to extract geometric relationship between domains.

The overall objective function of OSDA-ETD can be defined as follows:

$$\begin{aligned} \boldsymbol{g}^* = & \arg\min_{\boldsymbol{g}\in\mathcal{H}} R_s(\boldsymbol{g}) + \rho\|\boldsymbol{g}\|_k^2 + \gamma R_t^{u,C+1}(\boldsymbol{g}) - \sigma R_s^{u,C+1}(\boldsymbol{g}) + \\ & \lambda(1-\alpha) D_{\boldsymbol{g},k}^t(Q_s, Q_t^{\mathcal{Y}_s}) + \lambda\alpha \sum_{\hat{c}=1}^{C}\sum_{c=\hat{c}}^{C} D_{\boldsymbol{g},k}^t(Q_s^{\mathbf{x}_s|\mathbf{y}_c}, Q_t^{\mathbf{x}_t|\mathbf{y}_{\hat{c}}}) - \\ & \eta \sum_{\hat{c}=1}^{C}\sum_{c\neq\hat{c}} D_{\boldsymbol{g},k}^d(Q_s^{\mathbf{x}_s|\mathbf{y}_c}, Q_t^{\mathbf{x}_t|\mathbf{y}_{\hat{c}}}) + \mu R_m(\mathcal{D}_s, \mathcal{D}_t) \end{aligned} \tag{1}$$

where $\mathcal{H}$ is the hypothesis space, $R_s(\boldsymbol{g}) + \rho\|\boldsymbol{g}\|_k^2$ is the term of source domain structural risk, $R_t^{u,C+1}(\boldsymbol{g})$ and $R_s^{u,C+1}(\boldsymbol{g})$ are the risks that the samples are regarded as the unknown classes, $\gamma R_t^{u,C+1}(\boldsymbol{g}) - \sigma R_s^{u,C+1}(\boldsymbol{g})$ is the open set difference, $D_{\boldsymbol{g},k}^t(Q_s, Q_t^{\mathcal{Y}_s})$ represents the distribution discrepancy of inter-domain, $D_{\boldsymbol{g},k}^t(Q_s^{\mathbf{x}_s|\mathbf{y}_c}, Q_t^{\mathbf{x}_t|\mathbf{y}_{\hat{c}}})$ denotes the distribution difference of same class between different domains, $D_{\boldsymbol{g},k}^d(Q_s^{\mathbf{x}_s|\mathbf{y}_c}, Q_t^{\mathbf{x}_t|\mathbf{y}_{\hat{c}}})$ implies the distribution difference of different class between different domains, $R_m(\mathcal{D}_s, \mathcal{D}_t)$ represents the term of manifold regularization. In addition, $\lambda$, $\mu$, $\eta$, $\alpha$, $\gamma$, $\rho$, $\sigma$ are the parameters.

According to the representer theorem [27], the minimizer $\boldsymbol{g}^*$ in Eq. (1) is defined as:

$$\boldsymbol{g}^*(\mathbf{x}) = \sum_{i=1}^{n_s+n_t} \boldsymbol{\theta_i} K(\mathbf{x}_i, \mathbf{x}), \quad \forall \mathbf{x} \in \mathcal{X} \tag{2}$$

where $\mathbf{x}_i \in \mathcal{D}_s \cup \mathcal{D}_t$, $\boldsymbol{\theta}_i \in \mathbb{R}^{(C+1)\times 1}$ is the parameter and $K$ is the kernel. With the form of $\boldsymbol{g}^*$, in the following section, we will describe the computation of terms in Eq. (1).

### *C. Open set loss of OSDA-ETD*

In open set domain adaptation, our ultimate goal is to learn an adaptative model for the target domain. However, the target domain is composed of known and unknown classes, the identification of the unknown class is much more difficult than the known class. Fortunately, some incomplete multi-source domain adaptation works [28], [29] consider the recognition of unknown categories in the target domain. Recently, based on the open set learning

bound, DAOD enables the unknown target samples to be separated from samples using an open set difference. In our work, to identify the target domain samples as the corresponding known class and unknown class, following DAOD, we connect the structural risk of the source domain and the open set difference to construct the open set loss of OSDA-ETD. In this process, we utilize two label matrix. The first label matrix $\mathbf{Y} \in \mathbb{R}^{(C+1)\times(n_s+n_t)}$ can be defined as follows:

$$\mathbf{Y}_{ij} = \begin{cases} 1, & \mathbf{x}_j \in \mathcal{D}_{s,i} \\ 0, & \text{otherwise} \end{cases} \quad \text{when } i \leq C \tag{3}$$

$$\mathbf{Y}_{ij} = \begin{cases} 1, & \mathbf{x}_j \in \mathcal{D}_{t,C+1} \\ 0, & \text{otherwise} \end{cases} \quad \text{when } i = C+1 \tag{4}$$

where $D_{s,i}$ denotes the set of source samples in the $i-$th class and $D_{t,C+1}$ denotes target samples.

The other label matrix $\tilde{\mathbf{Y}} \in \mathbb{R}^{(C+1)\times(n_s+n_t)}$ is

$$\tilde{\mathbf{Y}}_{ij} = 1 \quad \text{iff} \quad i = C+1 \quad \text{and} \quad \mathbf{x}_j \in \mathcal{D}_s, \text{ otherwise } \tilde{\mathbf{Y}}_{ij} = 0 \tag{5}$$

Based on label matrix $\mathbf{Y}$ and $\tilde{\mathbf{Y}}$, the open set loss in OSDA-ETD can be defined as:

$$\begin{aligned} & R_s(\boldsymbol{g}) + \gamma R_t^{u,C+1}(\boldsymbol{g}) - \sigma R_s^{u,C+1}(\boldsymbol{g}) + \rho \|\boldsymbol{g}\|_k^2 \\ = & \|(\mathbf{Y} - \boldsymbol{\theta}^T\mathbf{K})\mathbf{B}\|_F^2 - \sigma \|(\tilde{\mathbf{Y}} - \boldsymbol{\theta}^T\mathbf{K})\tilde{\mathbf{B}}\|_F^2 + \rho \operatorname{tr}(\boldsymbol{\theta}^T\mathbf{K}\boldsymbol{\theta}) \end{aligned} \tag{6}$$

where $\boldsymbol{\theta} = [\boldsymbol{\theta_1}, \cdots, \boldsymbol{\theta_{n_s+n_t}}]^T \in \mathbb{R}^{(n_s+n_t)\times(C+1)}$, $\mathbf{B}$ and $\tilde{\mathbf{B}}$ are the $(n_s+n_t)\times(n_s+n_t)$ diagonal matrix, and $\mathbf{K}$ is a $(n_s+n_t)\times(n_s+n_t)$ kernel matrix. If $\mathbf{x}_i \in \mathcal{D}_s$, then $\mathbf{B}_{ii} = \sqrt{\frac{1}{n_s}}$ and $\tilde{\mathbf{B}}_{ii} = \sqrt{\frac{1}{n_s}}$. If $\mathbf{x}_i \in \mathcal{D}_t$, then $\mathbf{B}_{ii} = \sqrt{\frac{\gamma}{n_t}}$ and $\tilde{\mathbf{B}}_{ii} = 0$.

Unfortunately, due to the distribution difference between the source domain and target domain, the model inferred by Eq.(6) can not generalize well to the target domain. In the next section, we will address this issue.

### *D. Transferability in OSDA-ETD*

In this section, following the literature [25], [30], we reduce the global inter-domain difference and the local intra-class discrepancy. Generally, reducing the distribution differences denotes improving transferability. However, for open set domain adaptation, the target domain includes unknown classes. If we directly increase transferability will generate a negative transfer. Therefore, we enhance transferability after excluding recognized unknown target samples. In this process, we utilize the target pseudo labels predicted by classifiers. In particular, we rethink transferability that involves inter-domain and intra-class transfer. In terms of enhancing the inter-domain transferability, we utilize the Maximum Mean Discrepancy (MMD) criteria to measure the distribution distance between $Q_s$ and $Q_t^{\mathcal{Y}_s}$, which can be achieved as follows:

$$\begin{aligned} D_{\boldsymbol{g},k}^t(Q_s, Q_t^{\mathcal{Y}_s}) = & \|\frac{1}{n_s}\sum_{i=1}^{n_s}\boldsymbol{g}(\mathbf{x}_{s_i}) - \frac{1}{n_t^k}\sum_{j=1}^{n_t^k}\boldsymbol{g}(\mathbf{x}_{t_j}^k)\|_{\mathcal{H}_K}^2 \\ = & \operatorname{tr}\left(\boldsymbol{\theta}^T\mathbf{K}\mathbf{M_0}\mathbf{K}\boldsymbol{\theta}\right) \end{aligned} \tag{7}$$

where $n_t^k$ is the number of predicted known target samples, $\mathbf{x}_{t_j}^k$ represents the predicted known target samples, and $\mathbf{M_0}$ can be expressed as:

$$\mathbf{M_0} = \begin{bmatrix} \mathbf{e}_s\mathbf{e}_s^T & \mathbf{e}_s\mathbf{e}_t^T \\ \mathbf{e}_t\mathbf{e}_s^T & \mathbf{e}_t\mathbf{e}_t^T \end{bmatrix} \tag{8}$$

where

$$\mathbf{e}_s = \frac{1}{n_s}\mathbf{I}_{n_s\times 1}^s, \mathbf{e}_t = \frac{1}{n_t^k}\mathbf{I}_{n_t\times 1}^t \tag{9}$$

In Eq. (9), all elements in $\mathbf{I}_{n_s\times 1}^s$ are one. For $\mathbf{I}_{n_t\times 1}^t$, only elements with known class are one, and the rest are zero.

For the intra-class transfer, we employ the class-wise MMD to approximately measure $Q_s^{\mathbf{x}_s|\mathbf{y}_c}$ and $Q_t^{\mathbf{x}_t|\mathbf{y}_{\hat{c}}}$, and it can be defined as follows:

$$\begin{aligned} &\sum_{\hat{c}=1}^{C}\sum_{c=\hat{c}}^{C} D_{\boldsymbol{g},k}^t(Q_s^{\mathbf{x}_s|\mathbf{y}_c}, Q_t^{\mathbf{x}_t|\mathbf{y}_{\hat{c}}}) \\ &= \sum_{\hat{c}=1}^{C}\sum_{c=\hat{c}}^{C} \|\frac{1}{n_s^c}\sum_{i=1}^{n_s^c}\boldsymbol{g}(\mathbf{x}_{s_i}^c) - \frac{1}{n_t^{\hat{c}}}\sum_{j=1}^{n_t^{\hat{c}}}\boldsymbol{g}(\mathbf{x}_{t_j}^{\hat{c}})\|_{\mathcal{H}_K}^2 \end{aligned} \tag{10}$$

where $n_s^c$ refers to the number of source samples with label $c$, $n_t^{\hat{c}}$ denotes the count of target samples with pseudo label $\hat{c}$, $\mathbf{x}_{s_i}^c$ and $\mathbf{x}_{t_j}^{\hat{c}}$ are the samples of class $c$.

For the convenience of calculation, following the literature [31], we utilize the one-hot coding label matrix to calculate the transferability of intra-class. In particular, the source domain and the predicted target domain one-hot coding label matrix are written as $\mathbf{Y}_s = [\mathbf{y}_{s,1}; \ldots; \mathbf{y}_{s,n_s}]$ and $\hat{\mathbf{Y}}_t = [\hat{\mathbf{y}}_{t,1}; \ldots; \hat{\mathbf{y}}_{t,n_t^k}]$, where $\mathbf{y}_{s,i} \in \mathbb{R}^{1\times C}$ and $\hat{\mathbf{y}}_{t,i} \in \mathbb{R}^{1\times C}$. Therefore, the Eq. (10) can be expressed as:

$$\sum_{\hat{c}=1}^{C}\sum_{c=\hat{c}}^{C} D_{\boldsymbol{g},k}^t(Q_s^{\mathbf{x}_s|\mathbf{y}_c}, Q_t^{\mathbf{x}_t|\mathbf{y}_{\hat{c}}}) = \mathrm{tr}\left(\boldsymbol{\theta}^T\mathbf{K}\mathbf{M_l}\mathbf{K}\boldsymbol{\theta}\right) \tag{11}$$

where

$$\mathbf{M_l} = \begin{bmatrix} \mathbf{A}_s\mathbf{A}_s^T & -\mathbf{A}_s\mathbf{A}_t^T \\ -\mathbf{A}_t\mathbf{A}_s^T & \mathbf{A}_t\mathbf{A}_t^T \end{bmatrix} \tag{12}$$

In Eq. (12), $\mathbf{A}_s$ and $\mathbf{A}_t$ can be expressed as follows:

$$\mathbf{A}_s = \left[\frac{\mathbf{Y}_s(:,1)}{n_s^1}, \cdots, \frac{\mathbf{Y}_s(:,C)}{n_s^C}\right] \tag{13}$$

$$\mathbf{A}_t = \left[\frac{\hat{\mathbf{Y}}_t(:,1)}{n_t^1}, \cdots, \frac{\hat{\mathbf{Y}}_t(:,C)}{n_t^C}\right] \tag{14}$$

where $\mathbf{Y}_s(:,c)$ and $\hat{\mathbf{Y}}_t(:,c)$ denote the $c$-th column of $\mathbf{Y}_s$ and $\hat{\mathbf{Y}}_t(:,c)$, respectively.

In this section, we consider the transferability from both global and local perspectives. However, the remote sensing image characteristics of high inter-class similarity determine that only considering the transferability will degrade the classification performance. In the next section, we address this problem.

### *E. Discriminability in OSDA-ETD*

In this section, to improve the classification performance, we explore the discriminability based on the remote sensing scene images peculiarity of large inter-class similarity. To achieve discriminability, we leverage class-wise MMD to enlarge the distance of different known class, which can be expressed as

$$\begin{aligned}
&\sum_{\hat{c}=1}^{C}\sum_{c\neq\hat{c}} D^{d}_{\boldsymbol{g},k}(Q_s^{\mathbf{x}_s|\mathbf{y}_c}, Q_t^{\mathbf{x}_t|\mathbf{y}_{\hat{c}}}) \\
&= \sum_{\hat{c}=1}^{C}\sum_{c\neq\hat{c}} \|\frac{1}{n_s^c}\sum_{i=1}^{n_s^c}\boldsymbol{g}(\mathbf{x}_{s_i}^c) - \frac{1}{n_t^{\hat{c}}}\sum_{j=1}^{n_t^{\hat{c}}}\boldsymbol{g}(\mathbf{x}_{t_j}^{\hat{c}})\|^2_{\mathcal{H}_K} \\
&= tr(\boldsymbol{\theta}^T\mathbf{KFK}\boldsymbol{\theta})
\end{aligned} \tag{15}$$

where

$$\mathbf{F} = \begin{bmatrix} \mathbf{F}_s\mathbf{F}_s^T & -\mathbf{F}_s\mathbf{F}_t^T \\ -\mathbf{F}_t\mathbf{F}_s^T & \mathbf{F}_t\mathbf{F}_t^T \end{bmatrix} \tag{16}$$

In Eq. (16), $\mathbf{F}_s$ and $\mathbf{F}_t$ can be defined as

$$\mathbf{F}_s = \Big[\mathbf{A}_s(:,1)\bullet(C-1), \cdots, \mathbf{A}_s(:,C)\bullet(C-1)\Big] \tag{17}$$

$$\mathbf{F}_t = \Big[\mathbf{A}_t(:,1:C)_{\hat{c}\neq 1}, \cdots, \mathbf{A}_t(:,1:C)_{\hat{c}\neq C}\Big] \tag{18}$$

where $\mathbf{A}_s(:,1)$ represents the 1st column of $\mathbf{A}_s$, $\mathbf{A}_s(:,1)\bullet(C-1)$ repeats $\mathbf{A}_s(:,1)$ for $C-1$ times, and $\mathbf{A}_t(:,1:C)_{\hat{c}\neq 1}$ is composed of the 1st to the $C$-th (except the 1st) columns of $\mathbf{A}_t$.

### *F. Manifold Regularization*

To learn the geometrical relation between the source domain and target domain, following the literature [25], [30], [32], OSDA-ETD employs the manifold regularization, which can be computed as follows:

$$\begin{aligned}
R_m(\mathcal{D}_s, \mathcal{D}_t) &= \sum_{i,j=1}^{n_s+n_t} \|\boldsymbol{g}(\mathbf{x}_i) - \boldsymbol{g}(\mathbf{x}_j)\|_2^2\,\mathbf{W}_{ij} \\
&= \sum_{i,j=1}^{n_s+n_t} \boldsymbol{g}(\mathbf{x}_i)\mathbf{L}_{ij}\boldsymbol{g}(\mathbf{x}_j)
\end{aligned} \tag{19}$$

where $\mathbf{x}_i, \mathbf{x}_j \in \mathcal{D}_s \cup \mathcal{D}_t$, $\mathbf{L} = \mathbf{D} - \mathbf{W}$ is the Laplacian matrix, $\mathbf{D}_{ii} = \sum_{j=1}^{n_s+n_t}\mathbf{W}_{ij}$ is the diagonal matrix, and $\mathbf{W}$ is the pair-wise affinity matrix. The pair-wise affinity matrix estimates the similarity between samples and it can be defined as follows:

$$\mathbf{W}_{ij} = \begin{cases} \mathrm{sim}(\mathbf{x}_i, \mathbf{x}_j), & \mathbf{x}_i \in \mathcal{N}_p(\mathbf{x}_j) \text{ or } \mathbf{x}_j \in \mathcal{N}_p(\mathbf{x}_i) \\ 0, & \text{otherwise} \end{cases} \tag{20}$$

where sim $(\mathbf{x}_i, \mathbf{x}_j)$ represents the similarity function, $\mathcal{N}_p(\mathbf{x}_i)$ denotes the set of $p$-nearest neighbors to point $\mathbf{x}_i$, and $p$ is parameter.

### G. Overall Reformulation of OSDA-ETD

Finally, we combine the Eq.(6), (7), (11), (15), and (19) to reformulte the optimization problem in Eq.(1), which can be achieved as follows:

$$\boldsymbol{\theta}^* = \underset{\boldsymbol{\theta}\in\mathbb{R}^{(n_s+n_t)\times(C+1)}}{\operatorname{argmin}} \mathcal{L}(\boldsymbol{\theta}) \tag{21}$$

where

$$\begin{aligned}\mathcal{L}(\boldsymbol{\theta}) = &\|(\mathbf{Y}-\boldsymbol{\theta}^T\mathbf{K})\mathbf{B}\|_F^2 - \sigma\|(\tilde{\mathbf{Y}}-\boldsymbol{\theta}^T\mathbf{K})\widetilde{\mathbf{B}}\|_F^2 \\ &+\operatorname{tr}(\boldsymbol{\theta}^T\mathbf{K}(\lambda(1-\alpha)\mathbf{M_0}+\lambda\alpha\mathbf{M_1}-\eta\mathbf{F}+\mu\mathbf{L})\mathbf{K}\boldsymbol{\theta})+\rho\operatorname{tr}(\boldsymbol{\theta}^T\mathbf{K}\boldsymbol{\theta})\end{aligned} \tag{22}$$

There are some negative term in $\mathcal{L}(\boldsymbol{\theta})$. Therefore, the optimizer by solving $\frac{\partial\mathcal{L}(\boldsymbol{\theta})}{\partial\boldsymbol{\theta}} = \mathbf{0}$ may be a maximum point or a saddle point. Excitingly, based on the literature [25], we prove that there exists a unique optimizer in $\mathcal{L}(\boldsymbol{\theta})$. It's worth noting that the optimize can be solved by $\frac{\partial\mathcal{L}(\boldsymbol{\theta})}{\partial\boldsymbol{\theta}} = \mathbf{0}$. In the next section, we discuss in detail.

**Algorithm 1** OSDA-ETD Algorithm.

**Input:**

Data: source domain data matrix $\mathbf{X}_s$, target domain data matrix $\mathbf{X}_t$, source domain label $\mathbf{Y}_s$;

Parameter: $\lambda, \sigma, \rho, \alpha, \gamma, \mu, \eta$, $p$, and iterations $T$;

Train the classifier OSNN$^{\text{CV}}$ utilizing $\mathbf{X}_s$ and $\mathbf{Y}_s$, then apply prediction on $\mathbf{X}_t$ to get the initial pseudo label $\tilde{\mathbf{Y}}_t$;

Calculate Laplacian matrix $\mathbf{L}$;

Choose kernel function and compute kernel matrix $\mathbf{K}$;

$i = 1$;

**while** $i < T + 1$ **do**

  Construct discriminability matrix $\mathbf{F}$ by Equations (13), (14) , (16) , (17) and (18) ;

  Compute $\mathbf{M_1}$ by Equations (12), (13), (14) ;

  Calculate $\mathbf{M_0}$ by Equations (8), (9);

  Update the pseudo labels by $\tilde{\mathbf{Y}}_t = \boldsymbol{\theta}^T K$;

  $i = i + 1$

**end while**

**Output:**

Predicted target labels $\tilde{\mathbf{Y}}_t$ and classifier $\boldsymbol{\theta}^T K$.

### H. Theoretical proof of the unique optimizer

In this section, we provide the theoretical proof for the optimizer of $\mathcal{L}(\boldsymbol{\theta})$, as shown in *Lemma 1*.

***Lemma 1:*** if the parameters $\sigma < 1$ , $\eta \leq \frac{\lambda\alpha}{C-1}$, and the kernel function $K$ is universal, then the $\mathcal{L}(\boldsymbol{\theta})$ has a unique optimizer. It can be written as follows:

$$\begin{aligned}\boldsymbol{\theta} = ((\mathbf{B}^2 - \sigma\tilde{\mathbf{B}}^2 + \lambda(1-\alpha)\mathbf{M_0} + \lambda\alpha\mathbf{M_1} - \eta\mathbf{F} + \mu\mathbf{L})\mathbf{K} + \rho\mathbf{I})^{-1} \\ (\mathbf{B}^2\mathbf{Y}^T - \sigma\tilde{\mathbf{B}}^2\tilde{\mathbf{Y}}^T)\end{aligned} \tag{23}$$

According to the literature [25], we prove the *Lemma 1* from three parts.

**Claim 1:**

$$\lim_{\|\boldsymbol{\theta}\|_{\ell^2} \to +\infty} \mathcal{L}(\boldsymbol{\theta}) = +\infty \tag{24}$$

In Eq. (22), it is obvious that

$$\operatorname{tr}(\boldsymbol{\theta}^T\mathbf{K}(\lambda(1-\alpha)\mathbf{M_0} + \lambda\alpha\mathbf{M_1} + \mu\mathbf{L})\mathbf{K}\boldsymbol{\theta}) + \rho\operatorname{tr}(\boldsymbol{\theta}^T\mathbf{K}\boldsymbol{\theta}) \geq 0 \tag{25}$$

Then, we assume that the following equation holds:

$$\operatorname{tr}(\boldsymbol{\theta}^T\mathbf{K}(\lambda\alpha\mathbf{M_1} - \eta\mathbf{F})\mathbf{K}\boldsymbol{\theta}) \geq 0 \tag{26}$$

To verify the hypothesis of Eq.(26), we directly discuss the relationship between matrix $\lambda\mu\mathbf{M_1}$ and $\eta\mathbf{F}$, the details are as follows:

$$\lambda\alpha\mathbf{A}_s{\mathbf{A}_s}^T - \eta\mathbf{F}_s{\mathbf{F}_s}^T = \lambda\alpha\mathbf{A}_s{\mathbf{A}_s}^T - \eta(C-1)\ \mathbf{A}_s{\mathbf{A}_s}^T \tag{27}$$

$$\lambda\alpha\mathbf{A}_t{\mathbf{A}_t}^T - \eta\mathbf{F}_t{\mathbf{F}_t}^T = \lambda\alpha\mathbf{A}_t{\mathbf{A}_t}^T - \eta(C-1)\mathbf{A}_t{\mathbf{A}_t}^T \tag{28}$$

$$-\lambda\alpha\mathbf{A}_s{\mathbf{A}_t}^T - (-\eta\mathbf{F}_s{\mathbf{F}_t}^T) > -\lambda\alpha\mathbf{A}_s{\mathbf{A}_t}^T \tag{29}$$

$$-\lambda\alpha\mathbf{A}_t{\mathbf{A}_s}^T - (-\eta\mathbf{F}_t{\mathbf{F}_s}^T) > -\lambda\alpha\mathbf{A}_t{\mathbf{A}_s}^T \tag{30}$$

From the Eq. (27) to the Eq. (30), we observe that if $\eta \leq \frac{\lambda\alpha}{C-1}$, then the Eq. (26) holds.

By combining the Eq. (25) and the Eq. (26), we can get the following formula:

$$\begin{aligned}&\operatorname{tr}(\boldsymbol{\theta}^T\mathbf{K}(\lambda(1-\alpha)\mathbf{M_0} + \lambda\alpha\mathbf{M_1} - \eta\mathbf{F} + \mu\mathbf{L})\mathbf{K}\boldsymbol{\theta}) \\ &+\rho\operatorname{tr}(\boldsymbol{\theta}^T\mathbf{K}\boldsymbol{\theta}) \geq 0\end{aligned} \tag{31}$$

Next, we consider the partial term of open set loss function:

$$\|(\mathbf{Y} - \boldsymbol{\theta}^T\mathbf{K})\mathbf{B}\|_F^2 - \sigma\|(\tilde{\mathbf{Y}} - \boldsymbol{\theta}^T\mathbf{K})\widetilde{\mathbf{B}}\|_F^2 \tag{32}$$

Since the kernel $\mathbf{K}$ is universal and $\sigma < 1$, the matrix $\mathbf{K}(\mathbf{B^2} - \sigma\widetilde{\mathbf{B}})\mathbf{K}$ is symmetric and positive definite. It can be achieved as follows:

$$\mathbf{K}(\mathbf{B}^2 - \gamma\tilde{\mathbf{B}}^2)\mathbf{K} = \mathbf{O}\boldsymbol{\Lambda}\mathbf{O^T} \tag{33}$$

where $\mathbf{O}$ is the orthogonal matrix and $\boldsymbol{\Lambda}$ is the diagonal matrix. Then

$$\begin{aligned}&\|(\mathbf{Y} - \boldsymbol{\theta}^T\mathbf{K})\mathbf{B}\|_F^2 - \sigma\|(\tilde{\mathbf{Y}} - \boldsymbol{\theta}^T\mathbf{K})\widetilde{\mathbf{B}}\|_F^2 \\ &= \operatorname{tr}[(\boldsymbol{\theta}^{\mathrm{T}}\mathbf{O})\boldsymbol{\Lambda}(\boldsymbol{\theta}^{\mathrm{T}}\mathbf{O})^{\mathrm{T}}] - 2\operatorname{tr}[(\mathbf{Y}\mathbf{B}^2\mathbf{K} - \sigma\tilde{\mathbf{Y}}\tilde{\mathbf{B}}^2\mathbf{K})\boldsymbol{\theta}] + m \\ &\geq \upsilon\operatorname{tr}[(\boldsymbol{\theta}^{\mathrm{T}}\mathbf{O})\mathbf{I}(\boldsymbol{\theta}^{\mathrm{T}}\mathbf{O})^{\mathrm{T}}] - O(\|\boldsymbol{\theta}\|_{\ell^2}) + m \\ &= \upsilon\operatorname{tr}[\boldsymbol{\theta}^{\mathrm{T}}\boldsymbol{\theta}] - O(\|\boldsymbol{\theta}\|_{\ell^2}) + m\end{aligned} \tag{34}$$

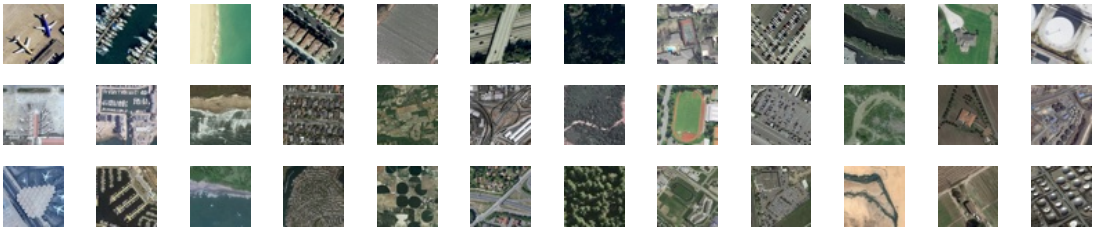

Fig. 3. Sample images of 12 common classes extracted from three data sets. Each column represents the corresponding categories of these data sets, from left to right are airfield, anchorage, beach, dense residential, farm, flyover, forest, game space, parking space, river, sparse residential, and storage cisterns. The top row to the bottom row are from the UC Merced data set, AID data set, and NWPU-RESISC45 data set.

where $\upsilon$ is the smallest diagonal element of the diagonal matrix $\mathbf{\Lambda}$, and $m$ is the constant.

Therefore

$$\begin{aligned} &\lim_{\|\boldsymbol{\theta}\|_{\ell^2}\to+\infty} \mathcal{L}(\boldsymbol{\theta}) \\ &\geq \lim_{\|\boldsymbol{\theta}\|_{\ell^2}\to+\infty} \upsilon\|\boldsymbol{\theta}\|_{\ell^2}^2 - O\left(\|\boldsymbol{\theta}\|_{\ell^2}\right) + m \\ &= +\infty \end{aligned} \tag{35}$$

**Claim 2:** There exists optimizers for $\mathcal{L}(\boldsymbol{\theta})$.

In claim 1, the Eq.(24) indicates that there have a constant $r > 0$, such that $\mathcal{L}(\boldsymbol{\theta}) > \mathcal{L}(0)$ for any $\boldsymbol{\theta} \in \mathbb{R}^{(n_s+n_t)\times(C+1)} \setminus B_r(0)$, where $B_r(0)$ is an open ball, $r$ denotes the radius of open ball, and the center of open ball is $\mathbf{0}$.

Due to $\mathcal{L}$ is a continuous function and the closed ball $\bar{B}_r(0)$ is a compact set, hence, there exist optimizers for $\mathcal{L}$ and these points belong to the $B_r(0)$ .

**Claim 3:** The optimizer of $\mathcal{L}(\boldsymbol{\theta})$ is unique.

If a point $\boldsymbol{\theta_0}$ is a minimizer, then

$$\frac{\partial \mathcal{L}}{\partial \boldsymbol{\theta_0}} = 0 \tag{36}$$

If the solution of Eq. (36) is unique, then the solution is the unique minimizer. The calculation of the Eq. (36) can be achieved as follows:

$$\begin{aligned} -2(\mathbf{K}\mathbf{B}^2\mathbf{Y}^T - \sigma\mathbf{K}\tilde{\mathbf{B}}^2\tilde{\mathbf{Y}}^T) + 2\rho\mathbf{K}\boldsymbol{\theta} + 2(\mathbf{K}\mathbf{B}^2\mathbf{K} - \sigma\mathbf{K}\tilde{\mathbf{B}}^2\mathbf{K})\boldsymbol{\theta} \\ +2\mathbf{K}(\lambda(1-\alpha)\mathbf{M_0} + \lambda\alpha\mathbf{M_1} - \eta\mathbf{F} + \mu\mathbf{L})\mathbf{K}\boldsymbol{\theta} = 0 \end{aligned} \tag{37}$$

The solution of Eq. (37) can be written as the Eq. (23).

Based on claim 1, claim 2, and claim 3, we illustrate that $\mathcal{L}(\boldsymbol{\theta})$ has a unique optimizer. The pseudocode of OSDA-ETD is provided in Algorithm 1.

## III. Experiments

In this section, we evaluate the effectiveness of OSDA-ETD. Firstly, we simply introduce the data sets. Next, we describe the experimental setup. After that, we show the experimental results . Finally, we discuss parameter sensitivity. Our code has been released.

TABLE II: CLASSIFICATION ACCURACY OF AID DATA SET AS SOURCE DOMAIN (%).

| Data set | Class | Methods | | | | | | |
|---|---|---|---|---|---|---|---|---|
| | | OSNN$^{CV}$ | TCA | SA | JDA | JPDA | DAOD | OSDA-ETD |
| AID→UC Merced | Airfield | 57.00 | 48.00 | 53.00 | 44.00 | **80.00** | 48.00 | 69.00 |
| | Anchorage | 55.00 | 49.00 | 55.00 | 61.00 | **65.00** | 55.00 | 55.00 |
| | Beach | **100.00** | **100.00** | **100.00** | **100.00** | **100.00** | **100.00** | **100.00** |
| | Dense Residential | 30.00 | 29.00 | 36.00 | 32.00 | 41.00 | 45.00 | **63.00** |
| | Farm | 23.00 | 25.00 | 31.00 | 43.00 | **80.00** | 32.00 | 45.00 |
| | Flyover | 2.00 | 4.00 | 8.00 | **58.00** | 0.00 | 7.00 | 7.00 |
| | Forest | 98.00 | 94.00 | 98.00 | **99.00** | 98.00 | 94.00 | 98.00 |
| | Game Space | 78.00 | 66.00 | 75.00 | 72.00 | 79.00 | 91.00 | **92.00** |
| | Parking Space | 98.00 | 98.00 | 94.00 | 98.00 | 98.00 | **100.00** | **100.00** |
| | Unknown | 46.67 | 48.00 | 49.00 | 43.00 | 42.67 | **75.67** | 70.00 |
| | OS* | 60.11 | 57.00 | 61.11 | 67.44 | **71.22** | 63.56 | 69.89 |
| | OS | 58.77 | 56.10 | 59.90 | 65.00 | 68.37 | 64.77 | **69.90** |
| | ALL* | 60.11 | 57.00 | 61.11 | 67.44 | **71.22** | 63.56 | 69.89 |
| | ALL | 56.75 | 54.75 | 58.08 | 61.33 | 64.08 | 66.58 | **69.92** |
| AID→NWPU-RESISC45 | Airfield | 28.29 | 38.21 | 32.07 | 56.79 | 58.29 | 68.93 | **76.29** |
| | Anchorage | 81.29 | 82.57 | 81.71 | 81.29 | 85.29 | **98.29** | 98.00 |
| | Beach | 68.29 | 73.14 | 69.71 | 85.57 | 86.00 | 95.86 | **97.00** |
| | Dense Residential | 75.71 | 77.71 | 69.57 | 78.29 | 85.86 | 94.43 | **96.00** |
| | Farm | 71.00 | 66.29 | 67.36 | 79.29 | 74.79 | 80.36 | **92.00** |
| | Flyover | 50.71 | 56.71 | 53.29 | 90.43 | 86.00 | 97.43 | **97.71** |
| | Forest | 91.00 | 88.14 | 97.86 | 98.43 | 97.86 | 96.86 | **99.29** |
| | Game Space | 77.07 | 67.50 | 73.29 | 78.07 | 77.21 | **95.79** | **95.79** |
| | Parking Space | 64.29 | 69.57 | 65.86 | 76.43 | 74.57 | 87.57 | **89.43** |
| | Unknown | 53.19 | 56.19 | 51.19 | 46.86 | 39.86 | **94.05** | 82.19 |
| | OS* | 67.52 | 68.87 | 67.86 | 80.51 | 80.65 | 90.61 | **93.50** |
| | OS | 66.08 | 68.87 | 66.19 | 77.14 | 76.57 | 90.95 | **92.37** |
| | ALL* | 65.33 | 65.99 | 65.29 | 78.23 | 78.01 | 88.38 | **92.13** |
| | ALL | 62.90 | 64.03 | 62.47 | 71.95 | 70.38 | 89.51 | **90.14** |

### A. Data sets

To verify the performance of OSDA-ETD, we utilize the UC Merced data set, AID data set, and NWPU-RESISC45 data set to construct the cross-domain data sets. The details of these data sets are as follows:

*1) UC Merced [33]:* The UC Merced data set can be downloaded from the United States Geological Survey

TABLE III: CLASSIFICATION ACCURACY OF UC Merced DATA SET AS SOURCE DOMAIN (%).

| Data set | Class | Methods | | | | | | |
|---|---|---|---|---|---|---|---|---|
| | | OSNN$^{cv}$ | TCA | SA | JDA | JPDA | DAOD | OSDA-ETD |
| UC Merced→AID | Airfield | 11.67 | 13.61 | 13.89 | 13.61 | **34.72** | 2.78 | 4.44 |
| | Anchorage | 12.37 | 29.21 | 14.21 | 61.58 | 7.63 | 51.58 | **63.16** |
| | Beach | 89.75 | 84.75 | 93.25 | 91.75 | 93.25 | 98.50 | **99.50** |
| | Dense Residential | 33.90 | 28.78 | 40.24 | 34.39 | 68.54 | 87.56 | **91.71** |
| | Farm | 4.86 | 6.49 | 16.22 | 12.16 | **86.76** | 8.92 | 14.86 |
| | Flyover | 32.62 | 36.43 | 15.48 | **75.71** | 4.05 | 0.00 | 0.00 |
| | Forest | 88.00 | 82.80 | 94.00 | 92.80 | 97.60 | **99.20** | **99.20** |
| | Game Space | 69.85 | 52.27 | **76.36** | 60.30 | 68.18 | 55.76 | 64.55 |
| | Parking Space | 87.95 | 83.59 | 78.46 | 89.74 | 89.74 | 97.44 | **98.21** |
| | Unknown | 48.50 | **51.12** | 44.95 | 34.95 | 20.75 | 48.60 | 39.16 |
| | OS* | 47.89 | 46.44 | 49.12 | 59.12 | **61.16** | 55.75 | 59.51 |
| | OS | 47.95 | 46.91 | 48.71 | 56.70 | 57.12 | 55.03 | **57.48** |
| | ALL* | 48.52 | 45.93 | 49.78 | 58.63 | **60.16** | 54.62 | 58.85 |
| | ALL | 48.51 | 47.11 | 48.68 | 53.25 | 51.21 | 53.25 | **54.37** |
| UC Merced→NWPU-RESISC45 | Airfield | 33.07 | 33.36 | 29.79 | **45.64** | 34.36 | 38.50 | 40.36 |
| | Anchorage | 50.67 | 56.57 | 38.86 | 33.14 | 44.57 | 95.86 | **97.14** |
| | Beach | 68.71 | 71.14 | 72.43 | 92.43 | 96.71 | 95.86 | **97.43** |
| | Dense Residential | 67.71 | 58.57 | 56.86 | 68.86 | 75.00 | 86.29 | **89.71** |
| | Farm | 3.14 | 3.86 | 8.50 | 43.93 | **78.43** | 37.79 | 39.43 |
| | Flyover | 72.73 | 74.71 | 60.00 | 91.71 | **92.57** | 81.57 | 91.57 |
| | Forest | 97.14 | 89.43 | 99.00 | 99.00 | **99.57** | 98.86 | 99.43 |
| | Game Space | 60.14 | 52.14 | **78.57** | 60.14 | 58.71 | 70.57 | 75.29 |
| | Parking Space | 46.14 | 43.43 | 38.57 | 78.71 | 46.71 | 89.00 | **90.71** |
| | Unknown | 44.38 | 50.05 | 39.10 | 31.57 | 29.57 | **92.00** | 85.95 |
| | OS* | 55.67 | 53.69 | 53.62 | 68.17 | 69.63 | 77.14 | **80.12** |
| | OS | 54.55 | 53.33 | 52.17 | 64.51 | 65.62 | 78.63 | **80.70** |
| | ALL* | 49.79 | 48.18 | 49.95 | 63.61 | 66.51 | 70.10 | **73.01** |
| | ALL | 48.70 | 47.71 | 47.78 | 57.20 | 59.12 | 74.48 | **75.60** |

(USGS) National Map. This data set is composed of 21 land-use scene categories. Each class contains 100 images with a spatial resolution of 0.3 m and a size of 256× 256 pixels

*2) AID [34]:* The AID data set is collected from Google Earth imagery and has a number of 10000 images with a size of 600 × 600 pixels. These images are divided into 30 classes. In addition, the spatial resolution of the

TABLE IV: CLASSIFICATION ACCURACY OF NWPU-RESISC45 DATA SET AS SOURCE DOMAIN (%).

| Data set | Class | Methods | | | | | | |
|---|---|---|---|---|---|---|---|---|
| | | OSNN$^{\text{CV}}$ | TCA | SA | JDA | JPDA | DAOD | OSDA-ETD |
| NWPU-RESISC45→AID | Airfield | 55.00 | 59.44 | 60.00 | 63.33 | 68.61 | 89.44 | **94.44** |
| | Anchorage | 60.00 | 61.05 | 56.84 | 74.47 | 65.26 | 59.21 | **82.63** |
| | Beach | 90.75 | 88.50 | 93.75 | 90.25 | 90.00 | 92.50 | **99.50** |
| | Dense Residential | 75.85 | 75.61 | 80.49 | 81.22 | 83.17 | 84.88 | **93.17** |
| | Farm | 71.62 | 75.68 | 74.59 | 75.95 | 77.84 | 96.76 | **98.11** |
| | Flyover | 87.38 | 86.43 | 90.24 | 91.19 | 83.57 | 94.05 | **98.33** |
| | Forest | 94.40 | 90.00 | 97.20 | 97.20 | 98.00 | 97.60 | **100.00** |
| | Game Space | 57.73 | 62.42 | 61.36 | 76.36 | **84.55** | 70.30 | 76.67 |
| | Parking Space | 97.69 | 94.87 | 96.92 | 95.13 | 94.36 | 97.44 | **98.97** |
| | Unknown | 48.41 | 47.85 | 43.46 | 43.83 | 38.13 | **84.49** | 73.64 |
| | OS* | 76.71 | 77.33 | 79.04 | 82.79 | 82.82 | 86.91 | **93.54** |
| | OS | 73.88 | 74.39 | 75.49 | 78.89 | 78.35 | 86.67 | **91.55** |
| | ALL* | 75.00 | 75.96 | 77.42 | 82.06 | 82.58 | 85.33 | **92.09** |
| | ALL | 68.96 | 69.58 | 69.70 | 73.38 | 72.48 | 85.14 | **87.90** |
| NWPU-RESISC45→UC Merced | Airfield | **98.00** | 96.00 | **98.00** | 90.00 | 97.00 | 97.00 | 97.00 |
| | Anchorage | 91.00 | 91.00 | 92.00 | **94.00** | **94.00** | 82.00 | 82.00 |
| | Beach | 90.00 | 91.00 | 96.00 | 93.00 | **99.00** | 96.00 | 96.00 |
| | Dense Residential | 41.00 | 41.00 | 38.00 | **58.00** | 32.00 | 29.00 | 31.00 |
| | Farm | 55.00 | 56.00 | 52.00 | 46.00 | **59.00** | 33.00 | 34.00 |
| | Flyover | 95.00 | 93.00 | 90.00 | **97.00** | 88.00 | 89.00 | 89.00 |
| | Forest | 96.00 | 95.00 | 95.00 | **98.00** | 92.00 | 90.00 | 91.00 |
| | Game Space | 26.00 | 38.00 | 39.00 | 49.00 | **58.00** | 37.00 | 37.00 |
| | Parking Space | **98.00** | 96.00 | 94.00 | 96.00 | 89.00 | 94.00 | 94.00 |
| | Unknown | 43.00 | 44.33 | 42.67 | 40.67 | 42.00 | **72.67** | 71.33 |
| | OS* | 76.67 | 77.44 | 77.11 | **80.11** | 78.67 | 71.89 | 72.33 |
| | OS | 73.30 | 74.13 | 73.67 | **76.17** | 75.00 | 71.97 | 72.23 |
| | ALL* | 76.67 | 77.44 | 77.11 | **80.11** | 78.67 | 71.89 | 72.33 |
| | ALL | 68.25 | 69.17 | 68.50 | 70.25 | 69.50 | **72.08** | **72.08** |

image ranges from 8 m to about half a meter.

*3) NWPU-RESISC45 [35]:* The NWPU-RESISC45 data set includes 45 scene categories. Each class contains 700 images with a size of 256 $\times$ 256 pixels. The spatial resolution ranges from about 30 m to 0.2 m.

In the above three heterogeneous data sets, the same class may have different names due to they are labeled by

TABLE V: Common classes extracted from three data sets.

| Class | Data set | | |
|---|---|---|---|
| | UC Merced | AID | NWPU-RESISC45 |
| Airfield | 100 | 360 | 1400 |
| Anchorage | 100 | 380 | 700 |
| Beach | 100 | 400 | 700 |
| Dense Residential | 100 | 410 | 700 |
| Farm | 100 | 370 | 1400 |
| Flyover | 100 | 420 | 700 |
| Forest | 100 | 250 | 700 |
| Game Space | 100 | 660 | 1400 |
| Parking Space | 100 | 390 | 700 |
| River | 100 | 410 | 700 |
| Sparse Residential | 100 | 300 | 700 |
| Storage Cisterns | 100 | 360 | 700 |

different experts. Hence, following the literature [22], [36], we select 12 public classes from the three data sets to construct the cross-domain data sets. This means that there have 6 domain adaptation tasks: UC Merced → AID, UC Merced → NWPU-RESISC45, AID → UC Merced, AID → NWPU-RESISC45, NWPU-RESISC45 → UC Merced, NWPU-RESISC45 → AID. The category information of cross-domain data sets is shown in Table V and the sample images of cross-domain data sets are shown in Fig. 3. In addition, we make an open set protocol for the cross-domain scene data sets, which chooses the top nine categories as the shared classes in alphabetical order and the last three classes as unknown classes in the target domain.

### *B. Experimental Setup*

*1) Evaluation Metrics:* To evaluate the proposed method, we adopt known classes average accuracy (OS*), all classes average accuracy (OS), known classes overall accuracy (ALL*), all classes overall accuracy (ALL), and classes accuracy (CA) as the evaluation criteria based on former works [24], [37] and reality. The details are as follows:

$$\text{ALL}^* = \frac{|\mathbf{x}: \ \mathbf{x} \in \mathcal{D}_{tk} \wedge \hat{\boldsymbol{g}}(\mathbf{x}) = \mathrm{y}_k|}{|(\mathbf{x}, \mathrm{y}_k) : (\mathbf{x}, \mathrm{y}_k) \in \mathcal{D}_{tk}|} \tag{38}$$

$$\text{ALL} = \frac{|\mathbf{x} : \mathbf{x} \in \mathcal{D}_t \wedge \hat{\boldsymbol{g}}(\mathbf{x}) = \mathrm{y}|}{|(\mathbf{x}, \mathrm{y}) : (\mathbf{x}, \mathrm{y}) \in \mathcal{D}_t|} \tag{39}$$

$$\text{CA} = \frac{|\mathbf{x} : \mathbf{x} \in \mathcal{D}_t^i \wedge \hat{\boldsymbol{g}}(\mathbf{x}) = i|}{|\mathbf{x} : \mathbf{x} \in \mathcal{D}_t^i|} \tag{40}$$

$$\text{OS}^* = \frac{1}{C} \sum_{i=1}^{C} \frac{|\mathbf{x} : \mathbf{x} \in \mathcal{D}_t^i \wedge \hat{\boldsymbol{g}}(\mathbf{x}) = i|}{|\mathbf{x} : \mathbf{x} \in \mathcal{D}_t^i|} \tag{41}$$

$$\text{OS} = \frac{1}{C+1} \sum_{i=1}^{C+1} \frac{|\mathbf{x} : \mathbf{x} \in \mathcal{D}_t^i \wedge \hat{\boldsymbol{g}}(\mathbf{x}) = i|}{|\mathbf{x} : \mathbf{x} \in \mathcal{D}_t^i|} \tag{42}$$

where $\mathcal{D}_{tk}$ denotes the known samples in the target domain and $\mathcal{D}_t^i$ is the target samples of the $i$-th class.

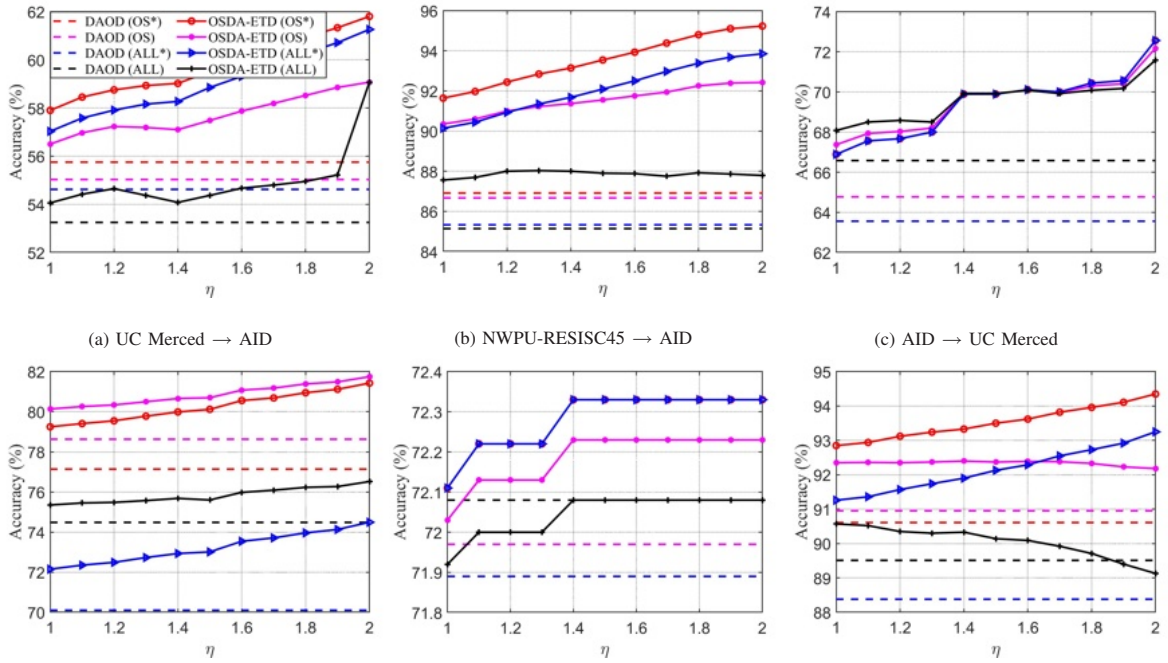


(a) UC Merced → AID (b) NWPU-RESISC45 → AID (c) AID → UC Merced

(d) UC Merced → NWPU-RESISC45 (e) NWPU-RESISC45 → UC Merced (f) AID → NWPU-RESISC45

Fig. 4. Effectiveness of discriminability on six cross data set.

*2) Implementation Detail:* To analyze the classification performance on the cross-domain data set, we leverage ResNet50 [38] to extract deep features from each image scene. In this paper, there have several parameters to set. As suggested in [30], we choose the Gaussian kernel as the kernel function. To balance the positive term $R^t_{u,C+1}(\boldsymbol{g})$ and the negative term $R^s_{u,C+1}(\boldsymbol{g})$ in the open set difference, we follow the rule of DAOD. In general, we set $\gamma = 0.4$ and $\sigma \in [0, 0.4]$. As for the other parameters $\lambda, \rho, p, \mu, T$, we also follow DAOD. Different from DAOD, OSDA-ETD considers the discriminability of inter-class. Therefore, we set the discriminability parameter is searched in $\eta \in [1, 1.1, 1.2, 1.3, 1.4, 1.5, 1.6, 1.7, 1.8, 1.9, 2.0]$.

*3) Compared Methods :* We compare the performance of OSDA-ETD with the following methods, which are:

- Open set Nearest Neighbor Class Verification (OSNN$^{\text{CV}}$) [39]: The OSNN$^{\text{CV}}$ is an open set classifier, which identifies unknown classes and known classes based on the labels consistency of test samples and two nearest neighbor samples.
- Transfer Component Analysis (TCA) [40] +OSNN$^{\text{CV}}$: TCA aligns the global distribution discrepancy between domains by using MMD, which is designed for closed set domain adaptation. In this paper, we only replace classifiers.
- Subspace Alignment [41]+OSNN$^{\text{CV}}$: SA aligns the subspace between domains by learning a mapping function. To implement SA in open set domain adaptation, we utilize OSNN$^{\text{CV}}$ as the classifier.
- Joint Distribution Adaptation (JDA) [42]+OSNN$^{\text{CV}}$: We extend JDA to the open set setting and try to reduce distribution discrepancy of known samples predicted by OSNN$^{\text{CV}}$.
- Joint Probability Domain Adaptation (JPDA) [43]+OSNN$^{\text{CV}}$: JPDA leverage discriminative joint probability

MMD to execute closed set domain adaptation. For the convenience of comparison, we also extend JPDA into the open set setting.

- DAOD+OSNN$^{\mathrm{CV}}$: A baseline of OSDA-ETD.

### C. Experimental Results

*1) Results of AID as source domain:* The table II summarizes the results of AID → UC Merced and AID → NWPU-RESISC45, where the highest accuracy is boldfaced. In table II, we can discover that SA and TCA perform poorly, even worse than the standard classifier OSNN$^{\mathrm{CV}}$. The reason is that TCA and SA are designed for closed set domain adaptation. If we directly apply the two methods to open set domain adaptation, it will cause a negative transfer. In contrast, the experimental results of almost all all open set methods are superior to OSNN$^{\mathrm{CV}}$. This phenomenon implies that there have distribution differences between domains. More importantly, OSDA-ETD achieves the best performance of all classes overall accuracy. Compared with JDA and DAOD, OSDA-ETD exploits the discriminability of different classes thus can lead to better performance. Moreover, different from JPDA, OSDA-ETD emphasizes inter-domain transferability, which helps to implement intra-class transferability and inter-class discriminability. In table II, We also find that some open set domain adaptation methods are inferior to OSDA-ETD and DAOD. The reason is that they utilize the common space to reduce the distribution discrepancy, this may cause the known class and the unknown class to mix together. In DAOD and OSDA-ETD, the negative term $R^s_{u,C+1}(\boldsymbol{g})$ are utilized to solve the above-mentioned problem.

*2) Results of UC Merced as source domain:* To validate the robustness of OSDA-ETD, we perform experiments on UC Merced→AID and UC Merced→NWPU-RESISC45, the results are list in table III. As shown in table III, the average classification accuracy (OS*, OS) and the overall accuracy (ALL*, ALL) of OSDA-ETD are superior to DAOD. This phenomenon demonstrates the effectiveness of increasing discriminability. Furthermore, for recognizing all target samples, OSDA-ETD can achieve the highest classification accuracy among all methods. However, in UC Merced → AID, JPDA is better than OSDA-ETD in identifying known classes. The reason is that OSDA-ETD balances the recognition of known and unknown classes via the positive term $R^t_{u,C+1}(\boldsymbol{g})$ and the negative term $R^s_{u,C+1}(\boldsymbol{g})$.

*3) Results of NWPU-RESISC45 as source domain:* The experimental results on NWPU-RESISC45 → AID and NWPU-RESISC45 → UC Merced are reported in table IV. On the NWPU-RESISC45 → AID dataset, OSDA-ETD achieves good results in most classes, which verifies the effectiveness of our proposal. On NWPU-RESISC45 → UC Merced, JDA performs better than other methods in recognizing known class. For identifying unknown class, DAOD and OSDA-ETD gain a huge performance. Therefore, DAOD and OSDA-ETD achieve the highest overall accuracy (ALL) among all methods. In addition, the table IV shows that the average classification accuracy (OS*, OS) of OSDA-ETD is better than DAOD.

### D. Parameter Sensitivity

We implement experiments on six cross data sets, experimental results demonstrate that the OSDA-ETD performs better on most tasks. To further verify the effectiveness of discriminability, we conduct sensitivity analysis about

$\eta$, as shown in Fig. 4. To be specific, we investigate the sensitivity of $\eta$ in a range [1,2]. From Fig. 4, we can find that with the increase of $\eta$, the OS*, OS, ALL*, ALL are also improved in most data sets. This phenomenon indicates that discriminability is extremely important in remote sensing scene classification. In Fig. 4 (f), with the increase of $\eta$, the evaluation metrics of ALL* increases while ALL decreases. This phenomenon is caused by the low recognition rate of unknown samples. In Fig. 4 (f), we utilize the AID data set as the source domain to classify the samples in the NWPU-RESISC45 data set. Due to the complexity of AID and NWPU-RESISC45 data sets, the discriminability of unknown classes is difficult to measure. In the future, we will further optimize discriminability to improve the recognition rate of unknown classes. In addition, even though the ALL of OSDA-ETD is decreasing, most of the performance of OSDA-ETD is better than DAOD. Note that, we report the experimental results by fixing $\eta$ to 1.5 in this paper, which also demonstrates the potential of OSDA-ETD.

## IV. Conclusion

In this paper, we introduce a realistic open set domain adaptation setting in remote sensing image scene classification, where the target domain can contain the unknown classes. To realize open set domain adaptation, the OSDA-ETD algorithm is proposed. Specifically, based on the characteristics of remote sensing images, OSDA-ETD considers transferability and discriminability. To improve transferability, OSDA-ETD reduces the global and local discrepancy. For the discriminability, OSDA-ETD enlarges the difference of inter-class. Finally, we integrate the transferability and the discriminability into a framework. It is worth noting that we prove that the OSDA-ETD has a unique optimizer. Extensive experiments validate the superiority of the OSDA-ETD.

In the future, we will improve the accuracy of unknown classes and extend the OSTA-ETD to a more general domain adaptation.

## References

[1] Q. Wang, S. Liu, J. Chanussot, and X. Li, "Scene classification with recurrent attention of vhr remote sensing images," *IEEE Transactions on Geoscience and Remote Sensing*, vol. 57, no. 2, pp. 1155–1167, 2019.

[2] R. Cao, L. Fang, T. Lu, and N. He, "Self-attention-based deep feature fusion for remote sensing scene classification," *IEEE Geoscience and Remote Sensing Letters*, vol. 18, no. 1, pp. 43–47, 2021.

[3] G. Cheng, X. Xie, J. Han, L. Guo, and G.-S. Xia, "Remote sensing image scene classification meets deep learning: Challenges, methods, benchmarks, and opportunities," *arXiv preprint arXiv:2005.01094*, 2020.

[4] E. Othmana, Y. Bazi, N. Alajlan, H. Alhichri, and F. Melgani, "Using convolutional features and a sparse autoencoder for land-use scene classification," *International journal of remote sensing*, vol. 37, no. 10, pp. 2149–2167, 2016.

[5] X. Han, Y. Zhong, B. Zhao, and L. Zhang, "Scene classification based on a hierarchical convolutional sparse auto-encoder for high spatial resolution imagery," *International Journal of Remote Sensing*, 2016.

[6] Y. Liu and C. Huang, "Scene classification via triplet networks," *IEEE Journal of Selected Topics in Applied Earth Observations and Remote Sensing*, vol. 11, no. 1, pp. 220–237, 2017.

[7] J. Zhang, M. Zhang, B. Pan, and Z. Shi, "Semisupervised center loss for remote sensing image scene classification," *IEEE Journal of Selected Topics in Applied Earth Observations and Remote Sensing*, vol. 13, pp. 1362–1373, 2020.

[8] Y. Yuan, J. Fang, X. Lu, and Y. Feng, "Remote sensing image scene classification using rearranged local features," *IEEE Transactions on Geoscience and Remote Sensing*, vol. 57, no. 3, pp. 1779–1792, 2019.

[9] W. Han, R. Feng, L. Wang, and Y. Cheng, "A semi-supervised generative framework with deep learning features for high-resolution remote sensing image scene classification," *ISPRS Journal of Photogrammetry and Remote Sensing*, vol. 145, pp. 23–43, 2018.

[10] S. Xu, X. Mu, D. Chai, and X. Zhang, "Remote sensing image scene classification based on generative adversarial networks," *Remote sensing letters*, vol. 9, no. 7, pp. 617–626, 2018.

[11] G. Wang and P. Ren, "Delving into classifying hyperspectral images via graphical adversarial learning," *IEEE Journal of Selected Topics in Applied Earth Observations and Remote Sensing*, vol. 13, pp. 2019–2031, 2020.

[12] S. Xu, X. Mu, D. Chai, and S. Wang, "Adapting remote sensing to new domain with elm parameter transfer," *IEEE Geoscience and Remote Sensing Letters*, vol. 14, no. 9, pp. 1618–1622, 2017.

[13] L. Yan, R. Zhu, N. Mo, and Y. Liu, "Cross-domain distance metric learning framework with limited target samples for scene classification of aerial images," *IEEE Transactions on Geoscience and Remote Sensing*, vol. 57, no. 6, pp. 3840–3857, 2019.

[14] D. Tuia, C. Persello, and L. Bruzzone, "Domain adaptation for the classification of remote sensing data: An overview of recent advances," *IEEE Geoscience and Remote Sensing Magazine*, vol. 4, no. 2, pp. 41–57, 2016.

[15] M. Wang and W. Deng, "Deep visual domain adaptation: A survey," *Neurocomputing*, vol. 312, pp. 135–153, 2018.

[16] E. Othman, Y. Bazi, F. Melgani, H. Alhichri, N. Alajlan, and M. Zuair, "Domain adaptation network for cross-scene classification," *IEEE Transactions on Geoscience and Remote Sensing*, vol. 55, no. 8, pp. 4441–4456, 2017.

[17] N. Ammour, L. Bashmal, Y. Bazi, M. M. A. Rahhal, and M. Zuair, "Asymmetric adaptation of deep features for cross-domain classification in remote sensing imagery," *IEEE Geoscience and Remote Sensing Letters*, vol. 15, no. 4, pp. 597–601, 2018.

[18] W. Teng, N. Wang, H. Shi, Y. Liu, and J. Wang, "Classifier-constrained deep adversarial domain adaptation for cross-domain semisupervised classification in remote sensing images," *IEEE Geoscience and Remote Sensing Letters*, vol. 17, no. 5, pp. 789–793, 2020.

[19] S. Song, H. Yu, Z. Miao, Q. Zhang, Y. Lin, and S. Wang, "Domain adaptation for convolutional neural networks-based remote sensing scene classification," *IEEE Geoscience and Remote Sensing Letters*, vol. 16, no. 8, pp. 1324–1328, 2019.

[20] J. Zhang, J. Liu, B. Pan, and Z. Shi, "Domain adaptation based on correlation subspace dynamic distribution alignment for remote sensing image scene classification," *IEEE Transactions on Geoscience and Remote Sensing*, vol. 58, no. 11, pp. 7920–7930, 2020.

[21] M. M. Al Rahhal, Y. Bazi, T. Abdullah, M. L. Mekhalfi, H. AlHichri, and M. Zuair, "Learning a multi-branch neural network from multiple sources for knowledge adaptation in remote sensing imagery," *Remote Sensing*, vol. 10, no. 12, 2018.

[22] X. Lu, T. Gong, and X. Zheng, "Multisource compensation network for remote sensing cross-domain scene classification," *IEEE Transactions on Geoscience and Remote Sensing*, vol. 58, no. 4, pp. 2504–2515, 2020.

[23] H. Chen, M. Ye, L. Lei, H. Lu, and Y. Qian, "Semisupervised dual-dictionary learning for heterogeneous transfer learning on cross-scene hyperspectral images," *IEEE Journal of Selected Topics in Applied Earth Observations and Remote Sensing*, vol. 13, no. 6, pp. 3164–3178, 2020.

[24] K. Saito, S. Yamamoto, Y. Ushiku, and T. Harada, "Open set domain adaptation by backpropagation," in *Proceedings of the European Conference on Computer Vision (ECCV)*, 2018, pp. 153–168.

[25] Z. Fang, J. Lu, F. Liu, J. Xuan, and G. Zhang, "Open set domain adaptation: Theoretical bound and algorithm," *IEEE Transactions on Neural Networks and Learning Systems*, pp. 1–14, 2020.

[26] H. Liu, Z. Cao, M. Long, J. Wang, and Q. Yang, "Separate to adapt: Open set domain adaptation via progressive separation," in *Proceedings of the IEEE Conference on Computer Vision and Pattern Recognition*, 2019, pp. 2927–2936.

[27] M. Belkin, P. Niyogi, and V. Sindhwani, "Manifold regularization: A geometric framework for learning from labeled and unlabeled examples," *Journal of Machine Learning Research*, vol. 7, no. 85, pp. 2399–2434, 2006. [Online]. Available: http://jmlr.org/papers/v7/belkin06a.html

[28] Z. Ding, M. Shao, and Y. Fu, "Incomplete multisource transfer learning," *IEEE Transactions on Neural Networks and Learning Systems*, vol. 29, no. 2, pp. 310–323, 2018.

[29] T. Gong, X. Zheng, and X. Lu, "Cross-domain scene classification by integrating multiple incomplete sources," *IEEE Transactions on Geoscience and Remote Sensing*, pp. 1–12, 2020.

[30] J. Wang, W. Feng, Y. Chen, H. Yu, M. Huang, and P. S. Yu, "Visual domain adaptation with manifold embedded distribution alignment," in *Proceedings of the 26th ACM international conference on Multimedia*, 2018, pp. 402–410.

[31] W. Zhang and D. Wu, "Discriminative joint probability maximum mean discrepancy (djp-mmd) for domain adaptation," *arXiv*, pp. arXiv–1912, 2019.

[32] M. Long, J. Wang, G. Ding, S. J. Pan, and P. S. Yu, "Adaptation regularization: A general framework for transfer learning," *IEEE Transactions on Knowledge and Data Engineering*, vol. 26, no. 5, pp. 1076–1089, 2014.

[33] Y. Yang and S. Newsam, "Bag-of-visual-words and spatial extensions for land-use classification," in *Proceedings of the 18th SIGSPATIAL international conference on advances in geographic information systems*, 2010, pp. 270–279.

[34] G.-S. Xia, J. Hu, F. Hu, B. Shi, X. Bai, Y. Zhong, L. Zhang, and X. Lu, "Aid: A benchmark data set for performance evaluation of aerial scene classification," *IEEE Transactions on Geoscience and Remote Sensing*, vol. 55, no. 7, pp. 3965–3981, 2017.

[35] G. Cheng, J. Han, and X. Lu, "Remote sensing image scene classification: Benchmark and state of the art," *Proceedings of the IEEE*, vol. 105, no. 10, pp. 1865–1883, 2017.

[36] R. Adayel, Y. Bazi, H. Alhichri, and N. Alajlan, "Deep open-set domain adaptation for cross-scene classification based on adversarial learning and pareto ranking," *Remote Sensing*, vol. 12, no. 11, p. 1716, 2020.

[37] P. Panareda Busto and J. Gall, "Open set domain adaptation," in *Proceedings of the IEEE International Conference on Computer Vision*, 2017, pp. 754–763.

[38] K. He, X. Zhang, S. Ren, and J. Sun, "Deep residual learning for image recognition," in *Proceedings of the IEEE conference on computer vision and pattern recognition*, 2016, pp. 770–778.

[39] P. R. M. Júnior, R. M. De Souza, R. d. O. Werneck, B. V. Stein, D. V. Pazinato, W. R. de Almeida, O. A. Penatti, R. d. S. Torres, and A. Rocha, "Nearest neighbors distance ratio open-set classifier," *Machine Learning*, vol. 106, no. 3, pp. 359–386, 2017.

[40] S. J. Pan, I. W. Tsang, J. T. Kwok, and Q. Yang, "Domain adaptation via transfer component analysis," *IEEE Transactions on Neural Networks*, vol. 22, no. 2, pp. 199–210, 2010.

[41] B. Fernando, A. Habrard, M. Sebban, and T. Tuytelaars, "Subspace alignment for domain adaptation," *arXiv preprint arXiv:1409.5241*, 2014.

[42] M. Long, J. Wang, G. Ding, J. Sun, and P. S. Yu, "Transfer feature learning with joint distribution adaptation," in *Proceedings of the IEEE international conference on computer vision*, 2013, pp. 2200–2207.

[43] W. Zhang and D. Wu, "Discriminative joint probability maximum mean discrepancy (djp-mmd) for domain adaptation," in *2020 International Joint Conference on Neural Networks (IJCNN)*. IEEE, 2020, pp. 1–8.